Multi-objective Optimization of Rotational Magnetorheological Abrasive Flow Finishing Process

COIN Report Number 2023007

Pushpendra Gupta[1], Vidyapati Kumar[1], Dilip Kumar Pratihar[1*], Kalyanmoy Deb[2]

[1]Department of Mechanical Engineering, Indian Institute of Technology Kharagpur, West Bengal, India

[2]Electrical and Computer Engineering, Michigan State University, East Lansing, MI 48824, USA

[*]Corresponding author- dkpra@mech.iitkgp.ac.in

Abstract

The Rotational Magnetorheological Abrasive Flow Finishing (R-MRAFF) technique achieves uniform, nano-level mirror finishes with high material removal rates, distinguishing it from other nano-finishing methods by combining rotational motion and magnetorheological abrasive particles during the nano-finishing process. Regression analysis is conducted to assess the influence of input process parameters, namely extrusion pressure (P), finishing cycles (N), rotational speed of magnet (S), and mesh size of abrasive (M) on the responses like percentage improvement in surface roughness ($\%\Delta R_a$) and amount of material removed (MR). The obtained regression equations for $\%\Delta R_a$, and MR are then used to formulate a multi-objective optimization problem, which is solved by an elitist non-dominated sorting genetic algorithm. The final results revealed a trade-off between these two objectives. The higher P, N, and S levels effectively generated a trade-off for the better surface finish and a good MR. However, the lower levels of M are adequate for both the responses. The study's findings, particularly the identified optimal parameters' combinations, offer valuable insights for maximizing the potential of R-MRAFF, enabling the attainment of desired surface finish and material removal characteristics in a range of applications. This study can be extended to other complex manufacturing processes with multiple parameters and responses.

Keywords: Nano-finishing, R-MRAFF Technique, Multi-objective Optimization, NSGA-II, Optimal Process Parameters

2.1 Introduction

Nano-finishing, a cutting-edge surface refinement technique, meticulously eliminates a minute fraction of material from the surface, operating within the nano-meter range. This process produces a high-quality surface finish with excellent surface properties, particularly useful in the Electronic and Mechanical industries [1], [2]. Nano-finishing methods have various applications in multiple sectors, including aviation, automotive, biomedical, and electronics. In the realm of aviation engineering, impeccably polished copper mirrors find significant utility owing to their exceptional thermal conductivity and heat capacity. However, due to the inherent softness of copper, achieving nano-finishing on this material is highly difficult.

To attain the better surface finish (SF), researchers applied different magnetorheological (MaR) procedures [3]. Nano-finishing techniques are harnessed to enhance the surface finish of engine components, yielding substantial benefits such as enhanced fuel efficiency and reduced emissions. Nanotechnology has also been used in paints to protect automobiles from scratches and other damage over time. Nanotechnology is also applied to other body components, including but not limited to chassis, engines, tires, and drive trains [4]. Within the biomedical industry, nano-finishing plays a pivotal role in augmenting medical implants' surface finish, fostering improved biocompatibility, and significantly reducing rejection rates. It is required for the mating surfaces of biomedical implants such as shoulder, hip, knee, and ankle joints for appropriate functioning and longevity [5]. In the electronics industry, applying nano-finishing techniques is instrumental in enhancing electronic components' surface finish, culminating in notable improvements in reliability and overall performance. Nanotechnology has been applied to electronic components to enhance their performance and durability. Nanotechnology can improve the conductivity of materials used in electronic components, making them more efficient. Nanotechnology can also be used to create smaller and more powerful electronic devices. Figure 2.1 shows the different nano-finishing applications in various industries.

A plethora of nano-finishing techniques exist, encompassing chemical mechanical polishing, electrochemical polishing, electropolishing, magnetic field-assisted finishing, MaR finishing, magnetorheological abrasive flow finishing [6], [7], and the rotational magnetorheological abrasive flow finishing process (R-MRAFF) [8]. R-MRAFF represents a highly advanced method that harmonizes rotational motion with MaR abrasive flow machining, delivering meticulous surface finishing and precise material removal rates. By employing an MaR

fluid infused with abrasive particles and a rotating magnetic field, R-MRAFF effectively eradicates material from the workpiece's surface. Notably surpassing its predecessors, R-MRAFF grants superior control over the material removal rate and surface finish by harnessing the synergistic potential of rotational motion and MaR abrasive particles.

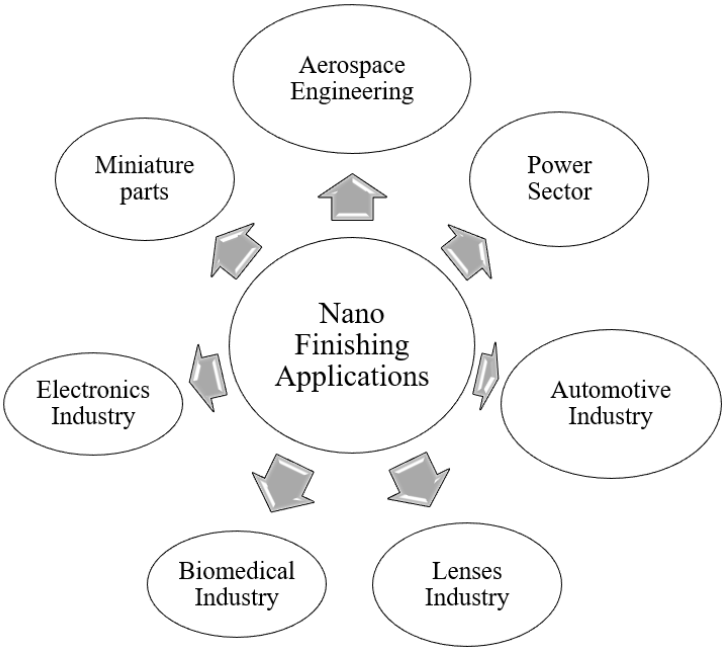

Figure 2.1 Applications of nano-finishing process in different industries.

The capability of generating superior surface finishes on diverse materials, including hard and brittle substances, has propelled the recent surge of interest in this process. Nonetheless, the optimization of process parameters for achieving the desired output responses in R-MRAFF remains a persistent challenge. To address this, the present study employs, elitist non-dominated sorting genetic algorithm-II (NSGA-II) [9], a well-established multi-objective optimization algorithm, in an endeavor to optimize the process parameters of R-MRAFF. A detailed discussion about the working of NSGA-II is given in Section 4. The considered process parameters are extrusion pressure (P) in bar, number of finishing cycles (N), rotational speed of the magnet (S) in RPM, and mesh size of abrasive (M). Meanwhile, the output responses under scrutiny are the final surface finish (SF) and material removal (MR). Regression analysis is employed to model their relationship to establish a connection between the process parameters and output responses. Initially, a real-coded genetic algorithm maximized one response by keeping the other as a constraint function. Later, both the responses are maximized using the NSGA-II algorithm and obtained Pareto-Front (PF) shows a clear trade-off between the SF and MR. The proposed

approach offers a significant advantage over traditional trial-and-error methods, as it significantly reduces the time and cost associated with optimizing the process parameters of R-MRAFF. Moreover, this approach could be easily extended to other complex manufacturing processes that involve multiple process parameters and output responses. Overall, this chapter aims to provide a comprehensive understanding of the R-MRAFF process and the use of an evolutionary algorithm to optimize its process parameters.

2.2 Rotational Magnetorheological Abrasive Flow Machining Process

The preceding section underscored the paramount importance of nano-finishing processes in attaining exceptional surface quality across various sectors. Numerous products' functional requirements necessitate achieving a nano-level surface finish. Nano-finishing processes can be broadly classified into magnetic field-assisted and non-assisted methods. Magnetic field-assisted techniques encompass magnetic abrasive finishing, MaR finishing, and similar methodologies, while non-assisted methods include abrasive flow finishing. Among the magnetic field-assisted methods, MRAFF stands out as a well-established technique capable of achieving nano-meter surface finishes on diverse materials, such as brass, aluminium, stainless steel, and silicon nitride. One modification that aids in attaining the desired nano-finishing level involves incorporating rotational motion into the MRAFF process. Figure 2.2 (a) illustrates the schematic view of an MRAFF experimental setup. Figure 2.2 (b) showcases the R-MRAFF process's mechanism, highlighting the magnets' rotational movement. Additionally, Figure 2.2 (c) depicts the alteration in rheological behaviour, specifically the changes in yield stress and viscosity, of the MaR-polishing fluid during the finishing process.

The quality of the finished surface in MaR fluid-based finishing processes is primarily influenced by the constituents of the MaR fluid and the applied magnetic field [11]. In their work, Sidpara and Jain [11] explored the correlation between rheological properties and surface finish quality in MaR fluid-based finishing processes. R-MRAFF employs a MaR fluid that possesses a distinctive characteristic of altering its viscosity and yield strength when it is subjected to a magnetic field. The magnetic field induces the formation of a microstructure within the fluid, enabling manipulation of the flow rate and direction. The presence of abrasive particles within the fluid facilitates the removal of material from the workpiece's surface. The concurrent rotation of

the magnetic field ensures an even distribution of the abrasive particles, resulting in a uniform surface finish.

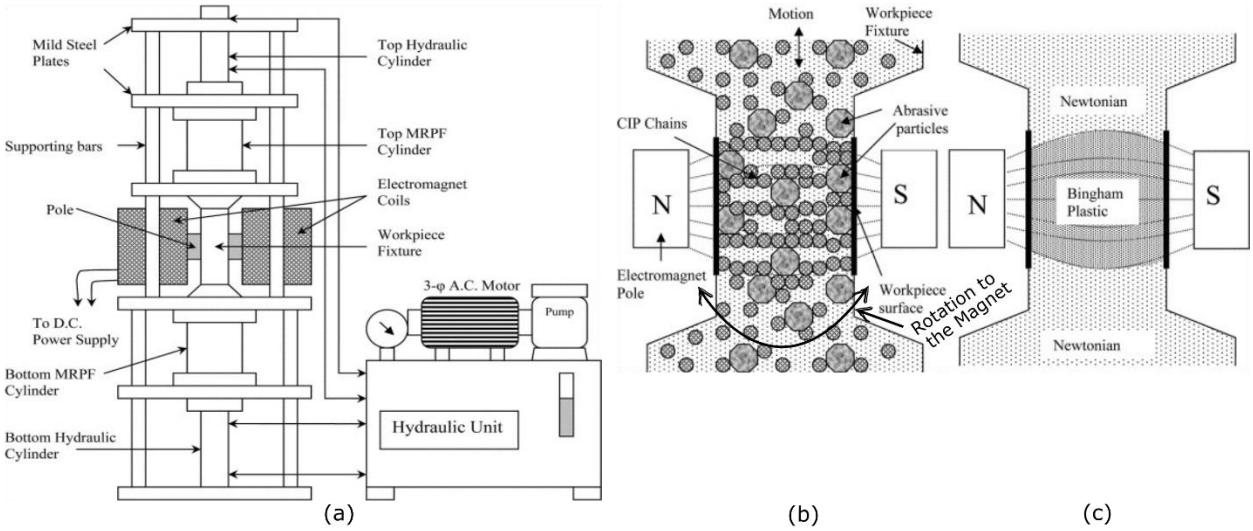

Figure 2.2 (a) A schematic representation of the experimental setup for MRAFF. (b) Mechanism of R-MRAFF process; (c) Observed changes in the rheological behaviour of the MaR-polishing fluid during the finishing process [10].

Consequently, the process utilizes a MaR fluid infused with abrasive particles and a rotating magnetic field to effectively eliminate material from the workpiece's surface. The distinctive amalgamation of rotational motion and MaR abrasive particles enables precise control over the material removal rate and surface finish, rendering it an ideal process for nano-finishing applications. R-MRAFF emerges as a significant nano-finishing technique, given its unparalleled ability to achieve high-quality surface finishes while ensuring precise control over the material removal rate. Compared to earlier processes, R-MRAFF offers enhanced control over the MR rate and SF, making it an appealing choice for accomplishing exceptional nano-level finishes.

2.3 Recent Developments in MRAFF Process

Rajput et al. [12] conducted a thorough examination of the different procedures and techniques used in MaR-fluid finishing processes and an assessment of their efficacy, too. The findings showed that this technique may produce extraordinary accuracy and surface quality without affecting the product's material topography. Karthikeyan et al. [13] investigated the in-vitro behaviour of stainless steel 316L treated to R-MRAFF in their investigation. They evaluated surface topography, roughness (Ra), and microhardness using experiments and analyses of treated

materials. Their results showed that the procedure improved surface quality, decreased roughness, and maintained or increased microhardness. These findings imply that the R-MRAFF technique has the potential to improve the performance of stainless-steel components in a variety of applications. In addition, Rajput et al. [14] devised a feature-based hybrid MRF planning system (FHMRF-PS) for the automated process planning of paraffin wax deposition in workpiece holes and pocket features prior to MRF. A case study on a Ti-6Al-4 V bone plate was performed to assess the efficiency and efficacy of the FHMRF-PS. The proposed process planning during MRF reduced the initial Ra value from 324.12 nm to 21.56 nm, illustrating the effectiveness of the designed FHMRF-PS.

Kumar et al. [15] discovered that an F-to-S iron ratio of 1:1, a DC supply of 12 V, a work sample rotating speed of 200 rpm, and a linear feed rate of 0.1 mm/min were the best parameter combinations for producing high-quality surfaces on S.S.-316 L cylindrical work samples. Karthikeyan et al. [16] elevated the hemocompatibility of SS 316L by lowering surface roughness and boosting surface energy during the R-MRAFF process. The required surface polish of SS 316L was attained using the following process parameters: 0.5-tesla magnetic field intensity, 10% abrasive concentration, and 200 revolutions per minute of rotating speed. Choopani et al. [17] encountered the effectiveness of the R-MRAFF technique in obtaining the requisite nano-finishing for Al2024 tubes. Surprisingly, they attained a Ra value of 26.3 nm and an MR value of 41 mg in just 15 minutes, demonstrating the efficiency of this method. Furthermore, Kumar et al. [18] implemented the R-MRAFF technique to obtain a minimum Ra of 34.5 nm and a maximum percentage increase in Ra ($\%\Delta R_a$) of 85.56% on a small steel gear. Furthermore, the finishing procedure efficiently removed the production flaws.

In light of the reviewed research, it becomes evident that MaR-fluid finishing techniques possess significant potential. These techniques demonstrate the ability to achieve exceptional precision, enhance surface quality, reduce roughness, and improve material performance across diverse applications. The optimization of process parameters emerges as a critical factor, enabling the attainment of desired surface finishes and the elimination of manufacturing flaws. Thus, it is crucial to gain a comprehensive understanding of and effectively control the variables involved in these processes to ensure favorable outcomes.

2.4 Elitist Non-dominated Sorting Genetic Algorithm-II

Elitist non-dominated sorting genetic algorithm II (NSGA-II) represents a state-of-the-art optimization algorithm rooted in evolutionary computing. Widely regarded as a benchmark technique in evolutionary computation, NSGA-II operates as a multi-objective optimization algorithm, enabling the simultaneous optimization of multiple objectives. Initially proposed by Deb et al. [9] in 2002 as an enhancement to the original NSGA algorithm, NSGA-II stands as a fast, efficient, and robust algorithm that has found extensive application in engineering, science, and economics. Its high efficiency and robustness make it an indispensable tool for optimizing complex systems and processes in industrial settings, capable of handling diverse optimization problems, including those involving non-linear and non-convex objective functions.

Unlike single-objective optimization algorithms that aim to discover a single optimal combination of design variables, a multi-objective optimization algorithm, such as NSGA-II, seeks to uncover multiple solutions known as Pareto optimal solutions. These solutions form a set of "non-inferior" solutions in the objective space, wherein further improvement in one objective necessitates a compromise in at least one of the other objectives. Addressing the needs of most industrial applications, NSGA-II tackles the simultaneous resolution of two or more conflicting objectives, generating better Pareto-optimal solutions. By minimizing two or three objectives concurrently and accommodating constraints, NSGA-II produces a Pareto optimal set with numerous solutions that optimize both objectives to such an extent that no other solution can enhance any objective without deteriorating another.

The primary advantage of NSGA-II lies in its capacity to identify a set of solutions that are non-dominated within the search space. Consequently, the algorithm discovers multiple solutions that are optimal in distinct ways rather than just a single optimal solution. This characteristic proves especially valuable in multi-objective optimization problems where the simultaneous optimization of multiple objectives is necessary, and no single solution can optimize all of them. The algorithm commences by generating an initial population of solutions evaluated based on their fitness in the search space. The fitness of a solution is determined by its ability to satisfy the various objectives of the optimization problem. Subsequently, the solutions are sorted into different levels of non-domination, with the first level consisting of solutions that are not dominated by any other solution, followed by subsequent levels containing solutions that are dominated by those in the preceding level, and so forth. After sorting the solutions, NSGA-II employs selection, crossover, and

mutation operators to generate a new population of solutions that remain non-dominated within the search space. This iterative process continues until optimal solutions are discovered or the maximum number of iterations is reached.

2.4.1 Working of NSGA-II

NSGA-II operates by maintaining a population of candidate solutions and iteratively guiding them toward improved outcomes, making it an exemplary algorithm for multi-objective optimization. One of its key strengths lies in its ability to converge toward the true Pareto-front, which is accomplished through the effective utilization of crossover and mutation operators. Crossover combines two chromosomes to create offspring, while mutation introduces random changes at the gene level. This interplay between crossover and mutation enables the population to converge while simultaneously reintroducing genetic diversity to steer clear of local minima. In addition to convergence, NSGA-II achieves other important qualities, such as maintaining a uniformly distributed and diverse set of solutions. These objectives are facilitated by the implementation of crowding distance. By employing an efficient crowding-distance assignment approach, NSGA-II ensures a well-spread population of solutions, while the employment of fast, non-dominated sorting enhances the algorithm's convergence capabilities. These advantages have propelled NSGA-II into wide-ranging applications and subjected it to numerous comparative studies, validating its performance. NSGA-II favors solutions with a higher crowding distance over other solutions within the same Pareto-front. It also incorporates the concept of elitism, where the best solutions are safeguarded and carried over to the next generation. These elite solutions are never eliminated and directly advance to the subsequent generation. The remaining solutions are compared amongst themselves, considering both their crowding distance and rank, to determine the most favorable solution. This ensures a fixed population size, as illustrated in Figure 2.3. Here, P_t is the set of solutions obtained in generation t, Q_t is the solution set obtained using crossover and mutation operators on P_t. Non-dominated sorting is performed after considering offspring and parent solutions to get different Pareto-fronts. Crowding distance is used to maintain the diversity of the solutions on each front.

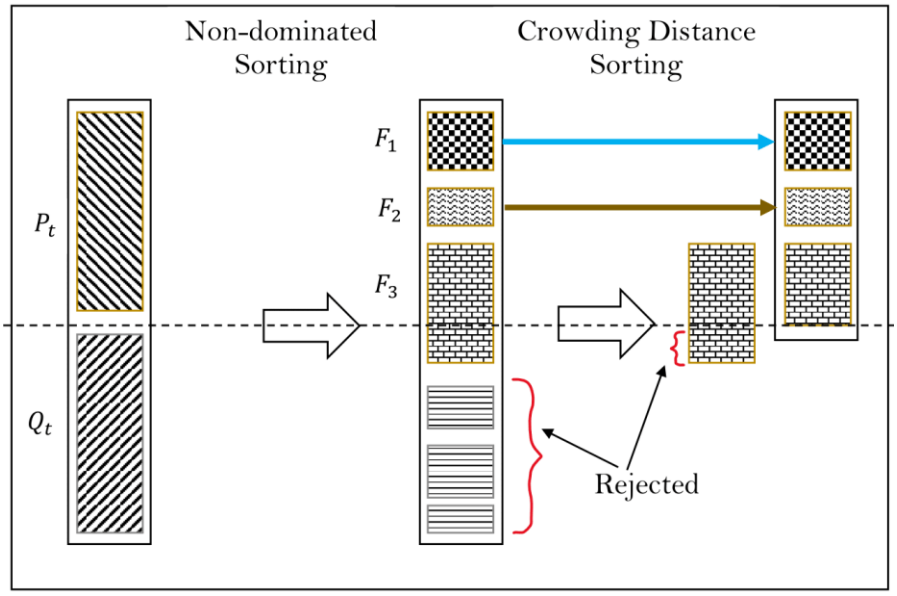

Figure 2.3 Working of NSGA-II.

To obtain the Pareto-front for multi-objective optimization, NSGA-II follows a step-by-step procedure:

1 Generate an initial random population, P.

2 Evaluate each solution to obtain the fitness function.

3 Perform non-dominated sorting based on non-domination criteria to find different PFs.

4 Calculate crowding distance to preserve diversity on each front.

5 Select individuals for the next generation based on their rank (lowest) and crowding distance (highest).

6 Generate new solutions, Q, from the previous generation using two operators, namely Crossover and Mutation.

The NSGA-II algorithm repeats steps 2 through 6 until a predefined stopping criterion is met. Typically, this criterion is either reaching the maximum number of generations or failing to obtain a better Pareto-front compared to the previous iteration.

2.5 Present Study

In various industrial sectors, the design of experiments (DOE) [19]–[23] is frequently employed for optimizing and developing manufacturing processes by examining the effect of multiple factors on a response. Das et al. [8] employed a DOE to evaluate the summary of responses, specifically MR and SF, using five levels of process parameters in their study on the R-MRAFF process. The

R-MRAFF method was utilized to finish the internal surface of cylindrical stainless steel (non-magnetic) workpieces. The central composite design (CCD) employed four factors with five levels, yielding a total of 30 experiments comprising 16 factorial runs, eight axial runs, and six center runs. The first parameter, hydraulic extrusion pressure (P) in bar, was varied across five levels, namely $32.5, 35, 37.5, 40$, and 42.5. The second parameter, the number of finishing cycles (N), ranged from $600, 800, 1000, 1200$, to 1400. The third parameter, the rotational speed of the magnet (S) in RPM, varied across $50, 100, 150, 200$, and 250. The fourth parameter, mesh size of abrasive (M), ranged from $90, 120, 150, 180$, to 210. Table 2.1 displays the responses, along with their various levels of process parameters considered during the experimental design.

Table 2.1 provided below includes measurements for both initial and final surface finishing (SF), and the percentage improvement in roughness denoted by $\%\Delta R_a$ as shown in the sixth column. Additionally, the material removal (MR) was calculated by weighing the samples before and after the machining process, with the difference between the two measurements indicating the amount of material removed in mg from the sample.

Table 2.1 Experimental results of R-MRAFF process on Surface Finish and Material Removal [8].

Run No.	Extrusion pressure, P (bar)	Finishing cycle, N	RPM magnet, S	Mesh size of SiC, M	Surface Finish (in $\%\Delta R_a$)	Material Removal (mg)
1	35	1200	100	120	90.00	12.3
2	40	1200	200	180	90.48	13.7
3	35	1200	200	180	81.08	8.1
4	37.5	1000	150	150	91.30	20.9
5	40	1200	200	120	91.89	23.5
6	40	800	200	180	74.29	7.3
7	40	800	100	180	87.23	11.4
8	37.5	600	150	150	81.08	6.8
9	37.5	1000	150	210	82.05	5.0
10	37.5	1000	150	150	90.91	25.1
11	37.5	1400	150	150	85.71	26.3

12	37.5	1000	150	150	90.00	23.2
13	42.5	1000	150	150	90.70	15.3
14	40	800	100	120	86.21	4.1
15	35	1200	200	120	80.00	24.0
16	37.5	1000	250	150	76.74	28.2
17	35	800	200	120	71.43	20.5
18	32.5	1000	150	150	75.86	8.1
19	40	1200	100	180	95.15	20.5
20	40	800	200	120	81.25	20.3
21	37.5	1000	50	150	82.22	5.1
22	37.5	1000	150	150	89.74	24.5
23	35	800	100	120	93.94	8.62
24	37.5	1000	150	150	85	20.5
25	37.5	1000	150	150	92.31	18.5
26	35	1200	100	180	92.17	19.9
27	40	1200	100	120	92.31	18
28	35	800	200	180	73.91	7.4
29	37.5	1000	150	90	88.24	27.8
30	35	800	100	180	85.29	11.5

2.6 Results and Discussion

Table 2.1 shows the SF and MR values obtained from the R-MRAFF experiments, which involved four factors at five levels using the CCD design. Figure 2.4 shows how the response variations are affected by each input parameter, using the mean values of both responses for a given process parameter level. During the increase in hydraulic pressure (*P*) from 32.5 to 35 bar and 35 to 37.5 bar, MR increased by 73.3% and 37.6%, respectively. Meanwhile, SF increased by 10.0% and 3.3%, respectively. However, further increasing P from 37.5 bar to 40 bar caused a decrease in MR by 23.2% and an increase in SF by 1.2%. Increasing P from 40 to 42.5 bar increased MR and SF by 3.0% and 3.8%, respectively. While increasing the number of finishing cycles (N) from 600

to 800 and 800 to 1000, MR increased by 67.5% and 62.56%, respectively, while SF increased by 0.75% and 5.5%. Increasing N from 1000 to 1200 caused a decrease in MR by 5.5% and an increase in SF by 3.3%.

Increasing N from 1200 to 1400 resulted in an increase in MR by 50.28% and a decrease in SF by 3.8%. When the magnet's rotational speed (S) is increased from 50 to 100 RPM, the MR increases significantly by 160.6%, while the improvement in SF is only 9.8%. As S is raised from 100 to 150 RPM, MR increased by 39.2%, but SF decreased by 3.7%. However, when S increased again from 150 to 200 RPM, MR and SF got worsened, declining by 15.7% and 7.32%, respectively. Conversely, when S is increased from 200 to 250 RPM, MR increases by 80.8%, but SF decreases by 4.7%. The increase in the Mesh size of the abrasive (M) from 90 to 120 has an adverse impact on both MR and SF, leading to a reduction of 41% and 2.7%, respectively. However, an increase in M from 120 to 150 resulted in an MR increase of 13%, while it barely affected the SF (almost 0.1%). Subsequently, an increase in M from 150 to 210 led to a decline in both MR and SF. The MR is decreased by 32% and 60%, respectively, while the SF is reduced by 1.2% and 3.4%, respectively.

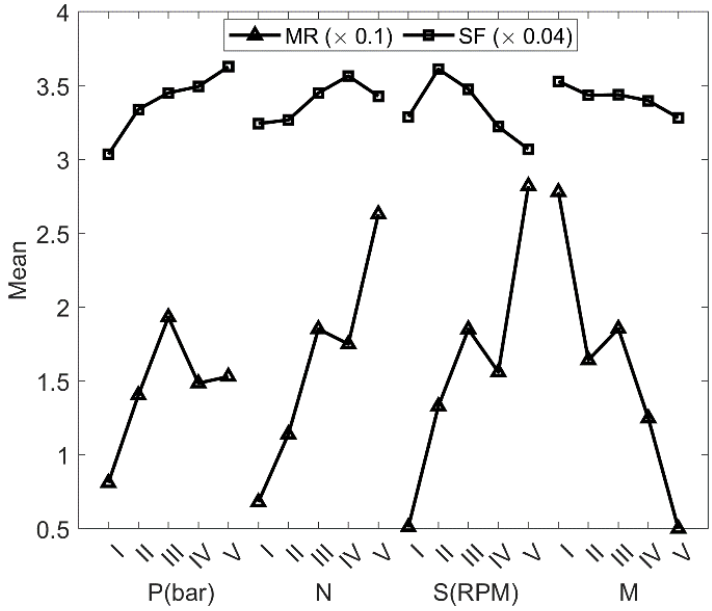

Figure 2.4 Effect of process parameters on response variation.

This analysis of experimental data examined the effects of the process parameters on the response variation, and it has been discovered that MR is more strongly affected than SF due to changes in process parameters. This is so because MR measured the total amount of material removed (in

mg) from the surface, while SF focused on surface finishing at a nano-level, which has minimal variation. The least effect on MR is observed due to parameter P, whereas the least impact on SF is observed due to parameter M. Parameter S has a significant effect on both MR and SF at different levels. If we consider the changes in responses caused by altering the process parameters to different levels, regardless of whether the responses increased or decreased, the order in which the parameters impacted MR from the least to the most is M, N, P, and S, while for SF it is M, N, P, and S.

2.6.1 Mathematical Modelling

The regression equation for MR and SF are developed, and the coefficient of determination (R^2) for both are found to be approximately 83.93% and 80.72%, respectively. Using regression analysis, the dependent variables MR and SF are modelled as non-linear functions of four independent process parameters, which are given in Equations (2.1) and (2.2).

$$MR = -688 + 30.4P + 0.0382N + 0.761S + 0.693M - 0.440\,P^2 - 0.000038\,N^2 - 0.000605S^2 - 0.001751\,M^2 + 0.00204\,PN + 0.00156\,PS + 0.0046\,PM - 0.000133\,NS + 0.000003\,NM - 0.003003\,SM \quad (2.1)$$

$$SF = -54 + 10.65\,P - 0.0804\,N - 0.560\,S + 0.111\,M - 0.195\,P^2 - 0.000030\,N^2 - 0.000867\,S^2 - 0.000835\,M^2 + 0.00277PN + 0.01599\,PS - 0.0013\,PM + 0.000160\,NS + 0.000175\,NM - 0.000091\,SM \quad (2.2)$$

The comparison between the present regression analysis and Das et al.'s [8] model is also shown in Figure 2.5. The MR equations are closely related and well-fitted to all experimental data. However, there is a significant difference in the SF equations, with Equation (2.2) fitting all experimental data closely, while the previous model barely passes through any data point. The present model has clearly outperformed the earlier model in terms of goodness of fit.

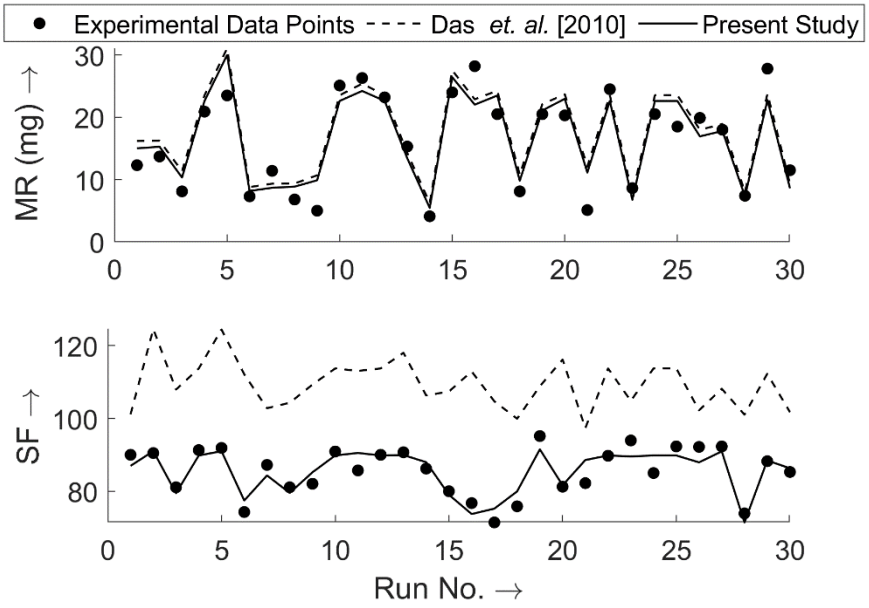

Figure 2.5 Comparison of the goodness of fit of the regression equations on the experimental data points between the present study and the study conducted by Das et al. [8].

2.6.2 Effect of Process Parameters on Responses

The variation of MR and SF with respect to the input parameters is shown in Figures 2.6 and 2.7, as response surface plots. The variation is shown concerning two independent values, while the other two are kept as constant. Figure 2.6(a) shows that MR initially increases with increasing pressure (P) and finishing cycles (N). However, MR eventually decreases with further increases in P and N. The maximum MR is found to occur when P and N are approximately equal to 37.5 bar and 1000, respectively. The other two parameters, the magnet's rotational speed (S) in RPM and mesh size (M) are kept fixed. Figure 2.6(b) shows that MR increases with the increasing S up to 200 RPM. After that, MR slightly decreases. N causes MR to increase exponentially at a fixed S (at 50 RPM). However, increasing S and N together causes MR to reduce further. Figure 2.6(c) shows that at a fixed M (around 100), the parameter S is found to be increasing the MR exponentially.

Similarly, at a fixed value to S (around 50 RPM), M is also found to be increasing the MR. However, the effect of S is found to be more compared to M. In the case of increasing both the parameters M and S, the MR is found to be decreased drastically; in fact, it reached a minimum.

Figure 2.6(d) shows that MR achieved an optimum value when P reached around 37.5 bar and M at around 160.

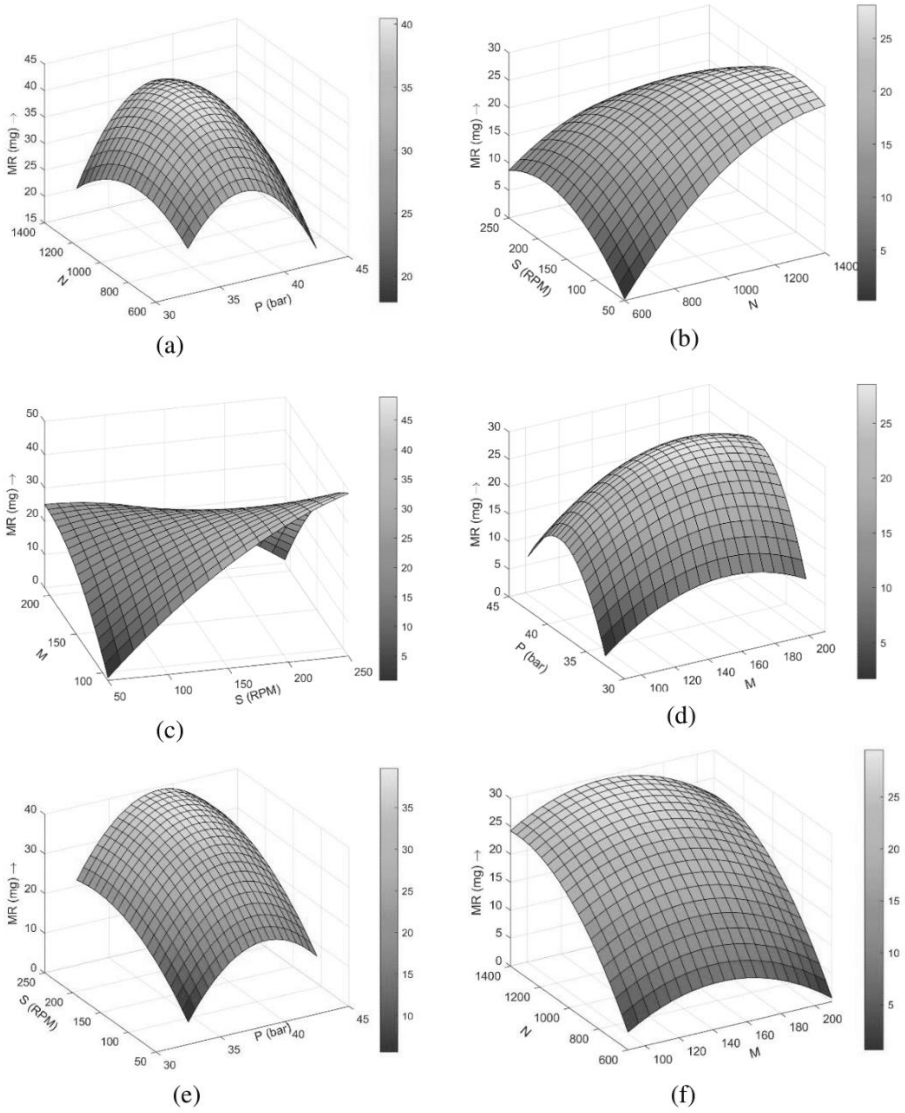

Figure 2.6 Effects of variation of process parameters on material removal.

Figure 2.6(e) shows a similar trend with respect to P. However, parameter S is found to be significantly helping in achieving the better MR with the higher value of S. Here, P is also found to assist in achieving the better MR at around 37.5 bar, and at this value of P, the parameter S further increases the MR with advancing its own value. Figure 2.6(f) shows a very similar trend with the parameters N and M, which was observed in Figure 2.6(e) with the parameters S and P, respectively. Here, the best value for M is found to be around 150, and N increases the MR by increasing its own value.

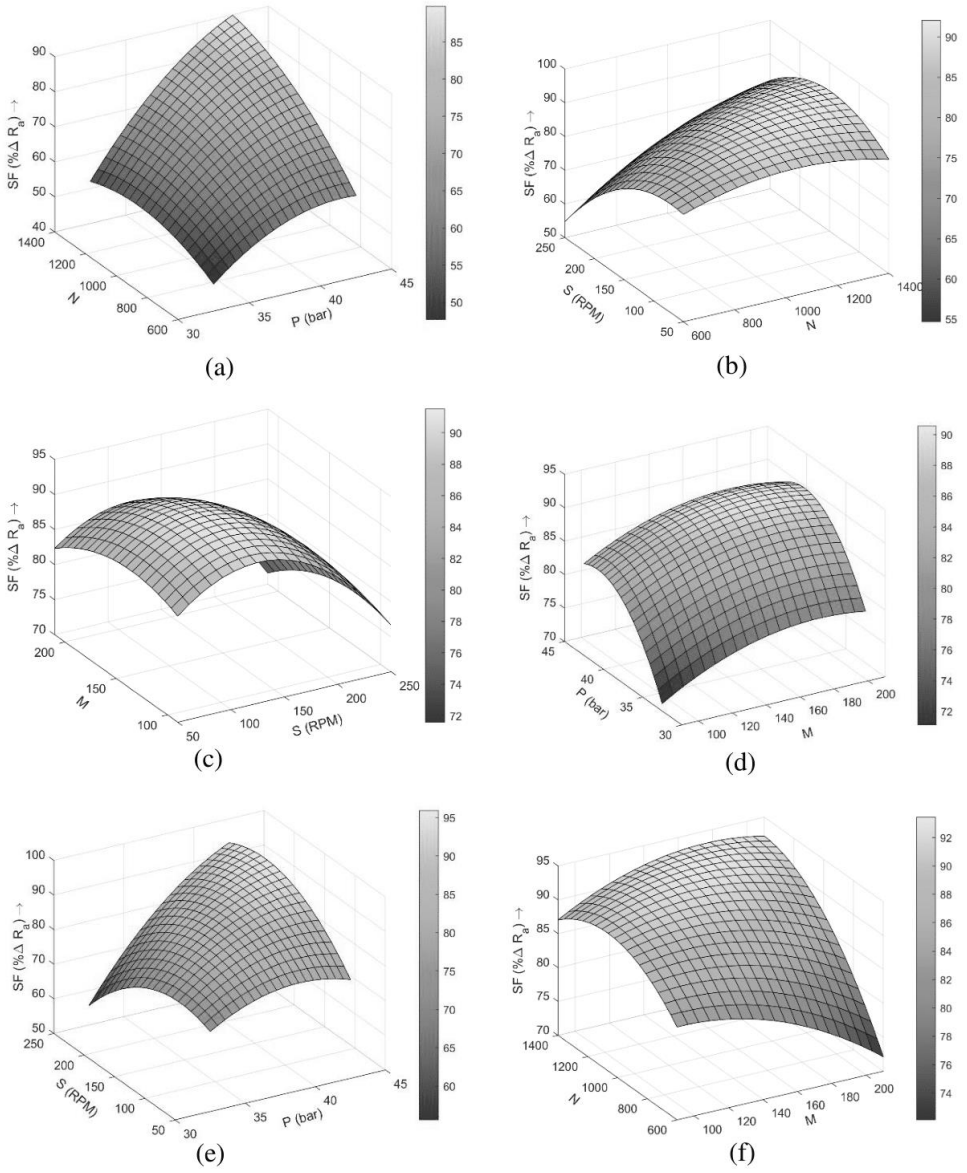

Figure 2.7 Effects of variation of process parameters on surface finish.

Similarly, Figure 2.7 shows the response surface plot for Surface Finish (SF). Figure 2.7(a) shows that the parameters P and N positively affect achieving the better surface finish. Figure 2.7(b) shows that the parameter S initially helps to attain the better SF but reduces it drastically later. At around S equals 150 RPM, SF seems to improve with the increasing N. Figure 2.7(c) shows that the parameter. M initially improves the SF and then reduces it. However, the parameter S shows a similar trend as mentioned in Figure 2.7(b), like at around S = 150 RPM, it enhances the SF. Figure 2.7(d) shows that when P is kept around 37.5 bar, the SF seems to improve with the increasing M,

provided that the rest of the parameters are kept fixed. Figure 2.7(e) shows that increasing S and P could help to obtain the better SF, while M and N are kept fixed. Figure 2.7(f) shows a similar trend with the parameters M and N. The results show that both MR and SF are complex functions of the input parameters.

2.6.3 Single-objective Optimization

The results of single-objective optimization using a real coded genetic algorithm [24] with a probability of crossover and mutation set to 0.9 and 0.3, respectively, are shown in Table 2.2. The population size and number of generations used are 200 and 500, respectively. Initially, SF is constrained to be at least 80%, while MR is maximized. The optimal values of the decision variables are found to be as follows: P = 39.14, N = 1175, S = 250, and M = 90. In the second attempt, SF is maximized while keeping MR as a constraint function. The constraint required a minimum material removal of 24 mg from the samples. The best combination of process parameters to achieve a 95.87% improvement in roughness is found to be as follows: P = 41.34, N = 1395, S = 182, and M = 137. This clearly demonstrates the trade-off between the two objective functions.

Table 2.2 Single-objective optimization results using a GA

Objective Functions (maximized)	Optimal Design Variables				Objective Functions	
	$P\ (bar)$	N	$S\ (RPM)$	M	$MR\ (mg)$	$SF\ (\%\Delta R_a)$
$MR\ (mg)$	39.14	1175	250	90	39.81	80.00
$SF\ (\%\Delta R_a)$	41.34	1395	182	137	24.00	95.87

However, these two solution sets represent the only options for prioritizing one objective function by keeping the other as a constraint. To visualize the trade-off better, the NSGA-II algorithm is used to identify a set of Pareto-optimal solutions that simultaneously maximize both MR and SF. NSGA-II is a population-based algorithm that searches for Pareto-optimal solutions iteratively.

2.6.4 Multi-objective Optimization

In nano-finishing operations, the goal is to achieve high levels of both surface finish (SF) and material removal (MR). However, these objectives can often conflict with each other. Increasing MR may result in a decrease in SF and vice versa. As a result, it is not possible to maximize both

objectives simultaneously. To address this trade-off, the NSGA-II algorithm is used to simultaneously maximize both MR and SF. The NSGA-II algorithm is designed to minimize the objectives by default. Therefore, the duality principle is used to convert the problem into a minimization problem by taking the reciprocal of MR and SF. The objectives are expressed using a quadratic mathematical model with four decision variables as given in Eqns (1) and (2). The NSGA-II multi-objective problem is formulated as follows:

$$\text{Minimize } \frac{1}{MR} \text{ (refer to Eqn (1))}$$

$$\text{Minimize } \frac{1}{SF} \text{ (refer to Eqn (2))}$$

with decision variables

$$P, N, S, \text{ and } M$$

subject to

$$32.5 \le P \le 42.5 \text{ (bar)},$$
$$600 \le N \le 1400,$$
$$50 \le S \le 250 \text{ (rpm)},$$
$$90 \le M \le 210$$

Out of the four decision variables, variation of pressure (P), is considered a real decision variable, while the rest are considered as integer decision variables. The multi-objective optimization problem described above is solved using NSGA-II with the following parameters:

Population Size = 200,

Number of Generations = 500,

Probability of Crossover = 0.9,

Probability of Mutation = 0.25,

Distribution Index for Crossover = 10, and

Distribution Index for Mutation = 20.

The Pareto-optimal solutions generated by NSGA-II are presented in Figure 2.8, which can be used to select the optimal machining parameters based on the decision maker's requirements. The most efficient solutions are enclosed within a rectangular box in Figure 2.8, as beyond that region in either direction, there is a higher sacrifice of one objective to achieve a marginal improvement in the other.

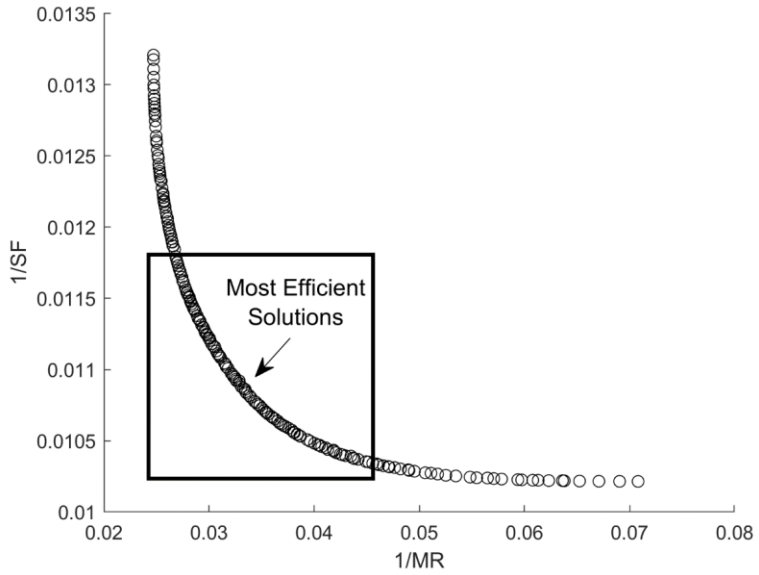

Figure 2.8 NSGA-II Pareto optimal solution set in objective space

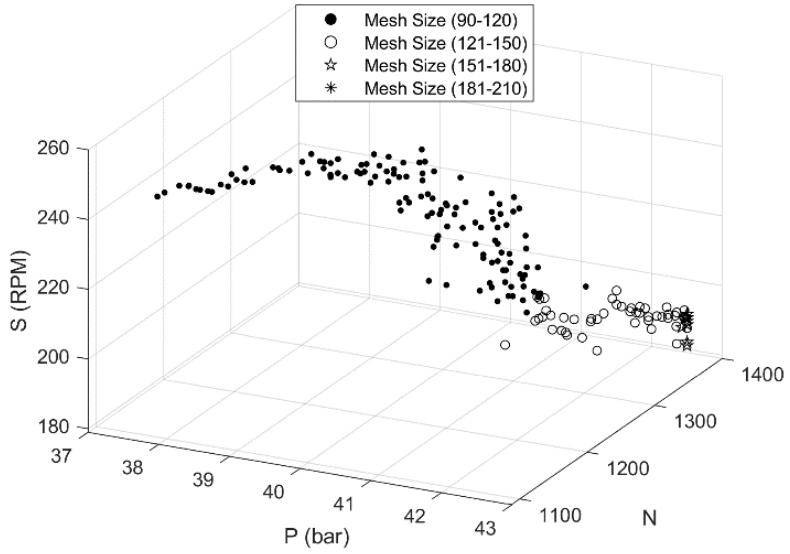

Figure 2.9 Variation of pressure (P), finishing cycles (N), magnet's rotation speed (S), and mesh size (M) in decision space.

The obtained Pareto-front, as shown in Figure 2.8, is found by the variation of decision parameters, which are shown in Figure 2.9. The graph's x, y, and z-axes represent the variation of parameters N, P, and S, respectively. The parameter M has been divided into four groups, namely 90-120,

121-150, 151-180, and 181-210. However, none of the solutions from the 181-210 group are identified, marked by an asterisk (*) in Figure 2.9.

It is observed that increasing the mesh size has a negative impact on both MR and SF. The relationship between the non-dominated solutions obtained using different decision variables can be better understood by examining Figure 2.9. It is evident that only a specific range of values for the parameter P (between 37 and 42.5 bar) significantly impacts both the objectives, whereas the initial two levels of P are not effective for either objective. The last two levels of N and S parameters are highly effective in achieving good SF and MR. These effects are further studied in detail using Figure 2.10.

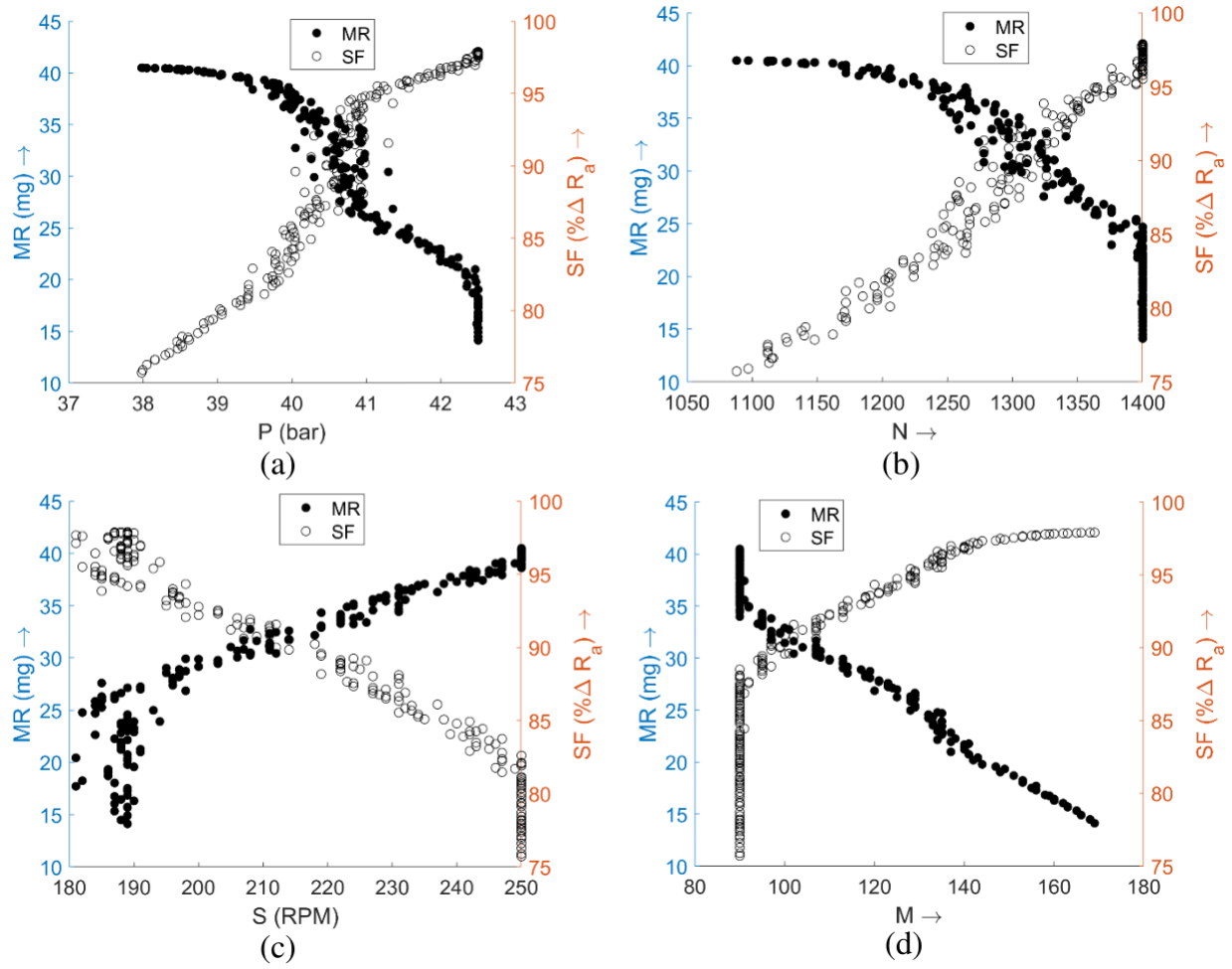

Figure 2.10 Effect of pressure (P), finishing cycles (N), magnet's rotation speed (S) and mesh size (M) on material removal (MR) and surface finish (SF).

Figure 2.10 displays the effects of P, N, S, and M parameters on MR and SF. Figure 2.10(a) reveals that when P is set to 37.5 bar, MR is maximized, but SF is poor. As P is increased, MR decreases, and SF improves. NSGA-II generates several solutions that can achieve good SF values close to 93% and MR values close to 32.5 mg at around 40.5 bar. SF enhanced with an increase in P, as the higher axial force facilitated material removal in the form of microchips. MR is increased due to the deeper penetration of abrasive particles into the workpiece surface, as the radial force is increased at the higher P [8]. However, MR has reached a maximum at an optimum value of 38 bar and then has decreased as the depth of penetration is reduced due to the shear-thinning nature of the MR Polishing Fluid. Figure 2.10(b) shows that the value of N that is good for both the objectives is approximately equal to 1300. Increasing N further reduces MR, but it improves SF. SF is enhanced with an increase in the parameter N due to a continuous enhancement in surface texture. However, the abrasive particles that initially cut the peaks of rough surfaces become worn out as N increases, and their effects on the polished surface are reduced due to increased hardness. Thus, it resulted in a poor amount of MR.

Figure 2.10 (c) shows that when S is kept equal to 210 RPM, MR and SF are both found to be good. However, increasing or decreasing S adversely affects both the objective functions. SF attains its maximum value at around 180 RPM of the parameter S. Beyond this value, SF is decreased, while MR increases. This trend can be attributed to increased tangential cutting force, which enhances MR. However, the centrifugal force acting on the abrasive particles indents the workpiece surface, resulting in a poorer SF [8]. Lastly, in Figure 2.10 (d), several solutions can attain a good SF value as high as 87.5% and MR close to 35 mg, even at a mesh size of 90. As the mesh size increases, only fewer solutions are available, resulting in a better surface finish but a poorer MR. Both SF and MR have improved at lower M. The higher M leads to more abrasives in the polishing medium due to a fixed concentration, and the abrasive diameter decreases at the larger mesh sizes. Consequently, the indentation force acting on each abrasive particle diminishes with increased mesh size, reducing the MR. However, SF has reached its maximum value at approximately 170 RPM.

2.7 Conclusion

R-MRAFF continues to emerge as an enticing choice for achieving exceptional nano-level surface finishes, boasting a uniform, smooth mirror-like surface (SF) with remarkable precision at the nano-meter scale. Moreover, this process exhibits an impressive capacity for higher material

removal (MR), surpassing the capabilities of preceding methods. By harnessing the synergistic effects of rotational motion and magnetorheological abrasive particles, R-MRAFF grants superior command over the material removal rate and surface finish, setting it apart as an advanced solution in the realm of nano-finishing techniques. The significance of R-MRAFF extends beyond its exceptional performance, as it enables the selective finishing of both internal and external surfaces on intricately shaped workpieces. Furthermore, this technique proves invaluable in situations where conventional finishing methods struggle to access and address specific areas. Consequently, its potential spans a wide array of industries that demand meticulous surface finishes on cylindrical components. Notably, sectors such as aerospace, automotive, and medical industries get the benefits significantly from the transformative capabilities of R-MRAFF.

In light of the comprehensive study conducted, the following conclusions have been drawn, shedding light on the optimal parameters and their corresponding outcomes:

- The optimal combination of parameters P, N, S, and M is found to be 39.14 bar, 1175 cycles, 250 rpm, and 90 mesh size, respectively, to achieve the highest MR of 39.81 mg, while SF is improved by around 80%.
- The optimal combination of process parameters to achieve SF of 95.87% is found when the parameters P, N, S, and M are set to 41.34 bar, 1395 cycles, 182 rpm, and 137 mesh size, respectively. The value of MR at the same parameter setting is found to be 24 mg.
- The higher levels of P, N, and S create a trade-off between improving the surface finish and obtaining a high MR. However, the lower levels of M are suitable for both responses. This can help the decision maker to select other combinations of process parameters for the desired result in SF and MR.
- Only a few solutions are able to improve SF at the expense of lower MR, which suggests that enhancing the surface finish is much more difficult than increasing the material removal using different combinations of parameters.

In summary, R-MRAFF emerges as an exceptionally promising approach for achieving superior nano-level surface finishes, surpassing previous processes in terms of uniformity, precision, and material removal efficiency. Its application potential spans diverse industries, including aerospace, automotive, and medical sectors, where high-quality surface finishes on cylindrical components are in high demand. Through the implementation of NSGA-II optimization, this study not only highlights the efficacy of R-MRAFF but also demonstrates the paramount importance of

optimizing process parameters to attain the desired surface finish and material removal outcomes. By combining the strengths of R-MRAFF and advanced optimization techniques, this research paves the way for advancements in surface finishing technology and opens new horizons for impeccable surface quality in various industrial applications.

References

[1] A. K. Singh, S. Jha, and P. M. Pandey, "Mechanism of material removal in ball end magnetorheological finishing process," *Wear*, vol. 302, no. 1–2, pp. 1180–1191, Apr. 2013, doi: 10.1016/J.WEAR.2012.11.082.

[2] S. Jha and V. K. Jain, "Modeling and simulation of surface roughness in magnetorheological abrasive flow finishing (MRAFF) process," *Wear*, vol. 261, no. 7–8, pp. 856–866, Oct. 2006, doi: 10.1016/J.WEAR.2006.01.043.

[3] H. Kansal, A. K. Singh, and V. Grover, "Magnetorheological nano-finishing of diamagnetic material using permanent magnets tool," *Precis Eng*, vol. 51, pp. 30–39, Jan. 2018, doi: 10.1016/J.PRECISIONENG.2017.07.003.

[4] J. Mathew, J. Joy, and S. C. George, "Potential applications of nanotechnology in transportation: A review," *J King Saud Univ Sci*, vol. 31, no. 4, pp. 586–594, Oct. 2019, doi: 10.1016/J.JKSUS.2018.03.015.

[5] T. S. Bedi, R. Kant, and H. Gurung, "Advanced Finishing Processes for Biomedical Applications," *Materials Horizons: From Nature to Nanomaterials*, pp. 105–126, 2022, doi: 10.1007/978-981-16-3645-5_5.

[6] A. Barman and M. Das, "Generation of Nano-Level Surface Finish by Advanced Nano-Finishing Processes," *Lecture Notes in Mechanical Engineering*, pp. 199–214, 2020, doi: 10.1007/978-981-15-2117-1_10/COVER.

[7] M. Kumar, A. Alok, V. Kumar, and M. Das, "Advanced abrasive-based nano-finishing processes: challenges, principles and recent applications," *https://doi.org/10.1080/10426914.2021.2001509*, vol. 37, no. 4, pp. 372–392, 2021, doi: 10.1080/10426914.2021.2001509.

[8] M. Das, V. K. Jain, and P. S. Ghoshdastidar, "NANO-FINISHING OF STAINLESS-STEEL TUBES USING ROTATIONAL MAGNETORHEOLOGICAL ABRASIVE FLOW FINISHING PROCESS," *http://dx.doi.org/10.1080/10910344.2010.511865*, vol. 14, no. 3, pp. 365–389, Jul. 2010, doi: 10.1080/10910344.2010.511865.

[9] K. Deb, A. Pratap, S. Agarwal, and T. Meyarivan, "A fast and elitist multiobjective genetic algorithm: NSGA-II," *IEEE Transactions on Evolutionary Computation*, vol. 6, no. 2, pp. 182–197, 2002, doi: 10.1109/4235.996017.

[10] S. Jha and V. K. Jain, “Design and development of the magnetorheological abrasive flow finishing (MRAFF) process,” *Int J Mach Tools Manuf*, vol. 44, no. 10, pp. 1019–1029, Aug. 2004, doi: 10.1016/J.IJMACHTOOLS.2004.03.007.

[11] A. Sidpara and V. K. Jain, “Rheological Properties and Their Correlation with Surface Finish Quality in MR Fluid-Based Finishing Process,” *http://dx.doi.org/10.1080/10910344.2014.925372*, vol. 18, no. 3, pp. 367–385, Jul. 2014, doi: 10.1080/10910344.2014.925372.

[12] A. S. Rajput, M. Das, and S. Kapil, “A comprehensive review of magnetorheological fluid assisted finishing processes,” *Machining Science and Technology*, vol. 26, no. 3. Taylor and Francis Ltd., pp. 339–376, 2022. doi: 10.1080/10910344.2022.2129982.

[13] S. Karthikeyan, B. Mohan, S. Kathiresan, and G. Anbuchezhiyan, “A study on in-vitro behaviour of stainless steel 316L subjected to rotational magnetorheological abrasive flow finishing process,” *Surf Topogr*, vol. 10, no. 3, Sep. 2022, doi: 10.1088/2051-672X/ac9150.

[14] A. Singh Rajput, S. Kapil, and M. Das, “Computer-aided process planning system for super finishing of flat surfaces with pockets through magnetorheological finishing process,” *Int J Comput Integr Manuf*, pp. 1–17, Mar. 2023, doi: 10.1080/0951192x.2023.2189313.

[15] V. Kumar, R. Kumar, and H. Kumar, “Development and investigation of the magnetorheological abrasive finishing (MRAF) system to nano-finish exterior cylindrical surfaces,” *Materials and Manufacturing Processes*, 2022, doi: 10.1080/10426914.2022.2072881.

[16] S. Karthikeyan, B. Mohan, S. Kathiresan, and G. Anbuchezhiyan, “Effect of process parameters on machinability, hemocompatibility and surface integrity of SS 316L using R-MRAFF,” *Journal of Materials Research and Technology*, vol. 15, pp. 2658–2672, Nov. 2021, doi: 10.1016/J.JMRT.2021.09.060.

[17] Y. Choopani, M. Khajehzadeh, and M. R. Razfar, “Experimental investigations into the nano-finishing of Al2024 tubes using the rotational-magnetorheological abrasive flow finishing (R-MRAFF) process,” *Proceedings of the Institution of Mechanical Engineers, Part E: Journal of Process Mechanical Engineering*, vol. 236, no. 6, pp. 2545–2557, Dec. 2022, doi: 10.1177/09544089221094999.

[18] M. Kumar, A. Kumar, H. N. S. Yadav, and M. Das, “Gear Profile Polishing Using Rotational Magnetorheological Abrasive Flow Finishing Process,” *Lecture Notes in Mechanical Engineering*, pp. 565–576, 2023, doi: 10.1007/978-981-19-3266-3_44/COVER.

[19] V. Kumar and S. Chakraborty, “Analysis of the Surface Roughness Characteristics of EDMed Components Using GRA Method,” 2022, pp. 461–478. doi: 10.1007/978-3-030-73495-4_32.

[20] A. Sharma, V. Kumar, A. Babbar, V. Dhawan, K. Kotecha, and C. Prakash, “Experimental Investigation and Optimization of Electric Discharge Machining Process Parameters Using Grey-Fuzzy-Based Hybrid Techniques,” *Materials*, vol. 14, no. 19, p. 5820, Oct. 2021, doi: 10.3390/ma14195820.

[21] V. KUMAR, P. P. DAS, and S. CHAKRABORTY, “Grey-fuzzy method-based parametric analysis of abrasive water jet machining on GFRP composites,” *Sādhanā*, vol. 45, no. 1, p. 106, Dec. 2020, doi: 10.1007/s12046-020-01355-9.

[22] V. Kumar, S. Diyaley, and S. Chakraborty, “Teaching-learning-based parametric optimization of an electrical discharge machining process,” *Facta Universitatis, Series: Mechanical Engineering*, vol. 18, no. 2, pp. 281–300, 2020, doi: 10.22190/FUME200218028K.

[23] S. Chakraborty, P. P. Das, and V. Kumar, “Application of grey-fuzzy logic technique for parametric optimization of non-traditional machining processes,” *Grey Systems: Theory and Application*, vol. 8, no. 1, pp. 46–68, 2018, doi: 10.1108/gs-08-2017-0028.

[24] S. Bandaru, R. Tulshyan, and K. Deb, “Modified SBX and adaptive mutation for real world single objective optimization,” *2011 IEEE Congress of Evolutionary Computation, CEC 2011*, pp. 1335–1342, 2011, doi: 10.1109/CEC.2011.5949771.